Annals of Glaciology 15 1991

Interannual characteristics of an 80 km resolution diagnostic Arctic ice–ocean model

JOHN E. RIES AND WILLIAM D. HIBLER, III
Thayer School of Engineering, Dartmouth College, Hanover, NH 03755, U.S.A.

ABSTRACT. Seasonal simulations with large-scale coupled ice–ocean models have reproduced many features of the ice and ocean circulation of the Arctic Ocean and the Greenland and Norwegian seas (e.g. Hibler and Bryan, 1987; Semtner, 1987). However, the crude resolution and high lateral eddy viscosity used by these models prevent the simulation of many of the smaller-scale seasonal features and tend to produce sluggish circulation. Similarly, the use of a single year's atmospheric forcing prevents the simulation of features on an interannual time-scale. As an initial step towards addressing these issues, an 80 km diagnostic Arctic ice–ocean model is constructed and integrated over a three-year period using daily atmospheric forcing to drive the model. To examine the effect of topographic resolution and eddy viscosity on model results, similar simulations were performed with a 160 km-resolution model. The results of these simulations are compared with one another, with buoy drift in the Arctic Basin, and with observed ice-edge variations. The model results proved most sensitive to changes in horizontal resolution. The 80 km results provided a more realistic and robust circulation in most areas of the Arctic and improved the modelled ice edge in the Barents Sea, while also successfully simulating the interannual variation in the region. Although it performed better than the 160 km model, the 80 km model still produced too large an ice extent in the Greenland Sea. No significant improvement in the ice-edge prediction was observed by varying the lateral eddy viscosity. The results indicate that problems remain in the vertical resolution in shallow regions, in treating penetrative convection, and in the simulation of inflow into the Arctic Basin through the Fram Strait.

INTRODUCTION

The importance of variations in Arctic ice extent to climatological studies has focused attention on the need to develop numerical models which reproduce the ice margins in the polar regions more realistically, especially in the Greenland, Iceland and Norwegian (GIN) seas. The dramatic seasonal change in this region requires an ice–ocean model with a resolution capable of simulating the physical mechanisms responsible for interannual ice-edge variations realistically. Specifically, a model needs to simulate effectively the heat transfer processes between the ice and ocean responsible for ice growth and decay, as well as the ocean circulation directly affecting the ice drift and dynamics.

Using a diagnostic ice–ocean model driven to seasonal equilibrium by daily 1979 atmospheric forcing, Hibler and Bryan (1987) obtained a more realistic ice-edge simulation in the East Greenland region than had previously been achieved. However, by using only a single year's forcing, the effect of interannual fluctuations of forcing and changes in the seasonal cycle could not be addressed. Moreover, Arctic Basin ice thicknesses were found to be excessive, as a result of the 1979 forcing fields that were used, and the simulated circulation in the Greenland Sea produced a relatively low northward heat transport, which was inadequate to balance the heat brought to the surface further north by convective overturning.

As an initial step towards addressing the issues of interannual variability and robustness of circulation, 80 km- and 160 km-resolution models of the Arctic Ocean and Greenland Sea have been constructed based on the ice–ocean model of Hibler and Bryan (1987). Analysis of this large-scale coupled model provides a means to examine large-scale seasonal and interannual variability of the simulated ice and ocean circulation in the Arctic and to investigate the physical processes responsible for ice-margin variations. To this end, the seasonal and interannual characteristics of the 80 km results are examined and compared to the results of a 160 km simulation, with specific attention to the Greenland and Barents seas region. The results are analyzed to determine whether changes in topographic resolution and lateral viscosity provide significant improvement to the modelled ocean circulation, ice edge, and ice drift.

https://doi.org/10.3189/1991AoG15-1-552-162 Published online by Cambridge University Press

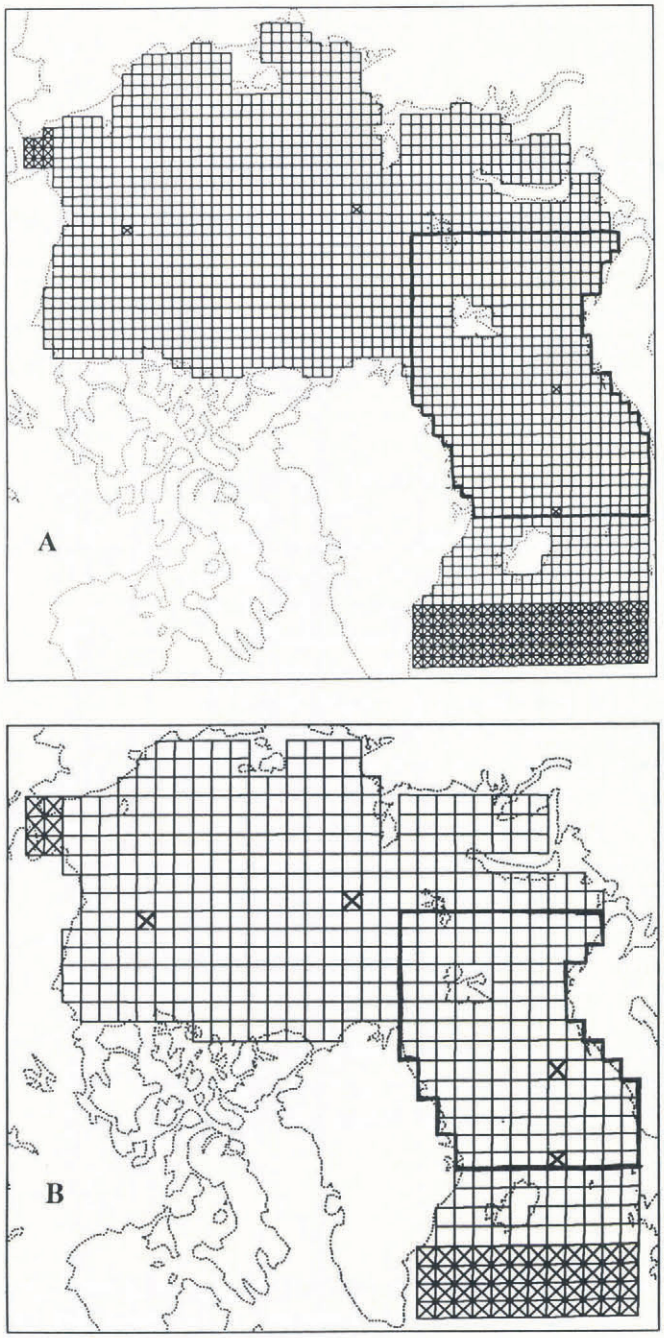

Fig. 1. (a) 80 km grid used for numerical simulations. (b) 160 km grid. Hatched areas represent regions where a 30 day relaxation to observed data is employed. The outlined area was used for more detailed time-series analysis. The grid cells marked by an "x" were used for stream-function analysis in Table 1.

MODEL DESCRIPTION

The coupled ice–ocean model of Hibler and Bryan (1987) consists basically of the two-level dynamic–thermodynamic sea-ice model of Hibler (1979), coupled to the multilevel baroclinic model of Bryan (1969). The sea-ice model provides heat, salt and momentum exchange boundary conditions for the top layer of the ocean, which itself provides current and heat exchange information as input to the ice model. To prevent long-term drift, the ocean is relaxed with a three-year time constant to the annual temperature and salinity estimates of Levitus (1982). The forcing fields driving the coupled model consist of daily atmospheric wind, mean monthly surface air temperature and humidity. These forcing fields were provided by John Walsh (personal communication). Observed ice extents used for comparison were extracted from monthly climatological data compiled by John Walsh (personal communication) from the Naval Polar Ocean Center's analyses.

An 80 by 80 km^2-resolution grid was constructed (Fig. 1), consisting of 65 by 66 grid cells. The Bering Strait and southern edge of the Greenland Sea are subjected to a 30 d diagnostic relaxation in the areas specified by the hatched grid cells in Figure 1. The Barents and GIN seas region used later for areal-averaged time-series analysis is denoted by solid black lines in the figure. Fourteen vertical levels are used in the ocean model and are the same as those used by Hibler and Bryan (1987). The model was integrated with a distorted time-stepping procedure using one-half day time steps for the ice model and for the ocean-model conservation equation. For the ocean-model momentum equations, a one-twentieth day time step was used. A one-year simulation requires approximately 20 hours of CPU time on one processor of an Alliant FX-40 mini-supercomputer as compared to two hours for the 160 km model, which was run at one day (and one-tenth day) time steps. All model simulations were performed by carrying out a two-year integration of the model with repeated 1980 forcing, followed by a three-year integration with a periodic forcing for the years 1981–83.

SIMULATION RESULTS AND DISCUSSION

Five separate simulations are treated in the following section. The two "standard" simulations are an 80 km simulation using a horizontal kinematic eddy viscosity of $0.5 \times 10^9\ cm^2\ s^{-1}$ and a 160 km simulation using a viscosity of $1.0 \times 10^9\ cm^2\ s^{-1}$. An ice-only simulation was run in which effects of the ocean model were removed by considering a fixed-depth motionless mixed layer and no ocean currents. However, daily average heat fluxes obtained from the standard 80 km simulation were used for this ice-only study. Two 80 km sensitivity studies using viscosities of 0.25×10^9 and $1.0 \times 10^9\ cm^2\ s^{-1}$ were also carried out to investigate the effects of lateral viscosity on the ocean circulation and ice margin.

Ice and ocean circulation characteristics

In Figure 2, a comparison of the March 1981 and August 1981 mean monthly stream-function for the standard 80 km and 160 km simulations is presented. These months represent extremes of the circulation over the three-year period (1981–83). A considerably more robust circulation is present in the 80 km model results. Especially notable is the improved circulation in the Greenland Sea region and the Eurasian Basin.

There is a quite prominent double-gyred circulation evident in the March stream-function of the 80 km model, with about 5 Sverdrups of flow clockwise in the central Arctic Basin and 5 Sverdrups counterclockwise in the Greenland Sea region. This can be compared with the

https://doi.org/10.3189/1991AoG15-1-552-162 Published online by Cambridge University Press

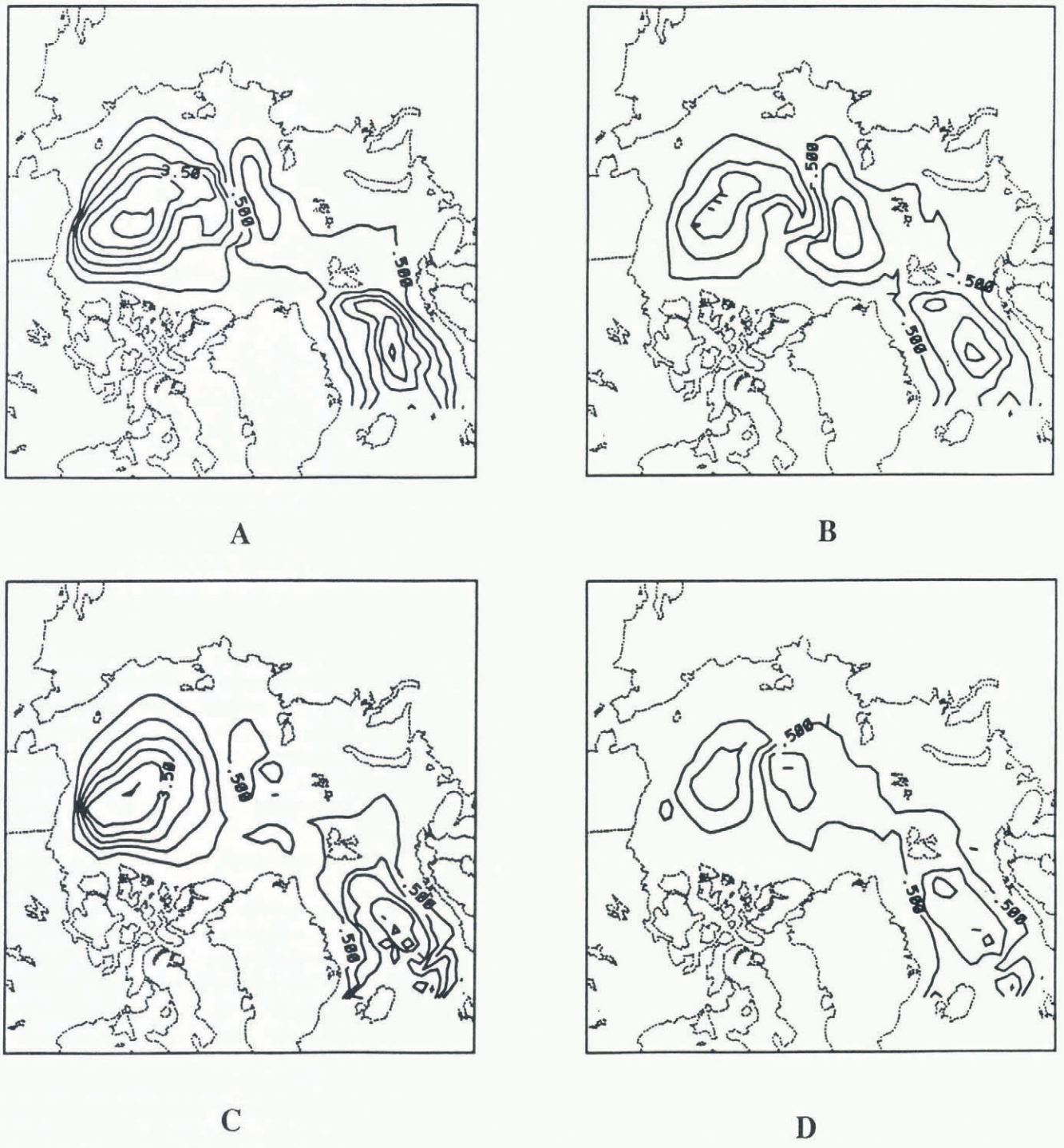

Fig 2. (a) March 1981 stream-function, 80 km standard simulation. (b) August 1981 stream-function, 80 km standard simulation. (c) March 1981 stream-function, 160 km standard simulation. (d) August 1981 stream-function, 160 km standard simulation. Contour lines are plotted at an interval of 1 Sverdrup.

160 km model with 4 Sverdrups of flow in the Arctic Basin and 3 Sverdrups of flow in the Greenland Sea. Present estimates of oceanic volume transport in the Arctic bracket the values of both models for the major basins. However, the 80 km model has excessive flow into the Barents Sea. This is likely to be caused by the inability of the model to simulate the West Spitsbergen Current accurately, redirecting some of the flow into the Barents Sea instead.

Comparison of the stream-functions with the mean monthly surface currents, from the second level of the 80 km ocean model (presented in Fig. 3), shows that the extremes occurring in March and August are largely barotropic in nature. Much of the change reflected occurs in the shallower water near the margins of the basin. The largest variations occur over the Siberian Shelf in the margin of the Beaufort Gyre. The currents modelled here are excessive, due to the low vertical resolution of the model, the effect of which is especially pronounced in the shallow shelf region. It appears that, where the currents would actually be redirected at the shallow shelf break, the model has unrealistically deep water. This is insufficient to redirect the flow, allowing large currents to flow onto the shelf.

https://doi.org/10.3189/1991AoG15-1-552-162 Published online by Cambridge University Press

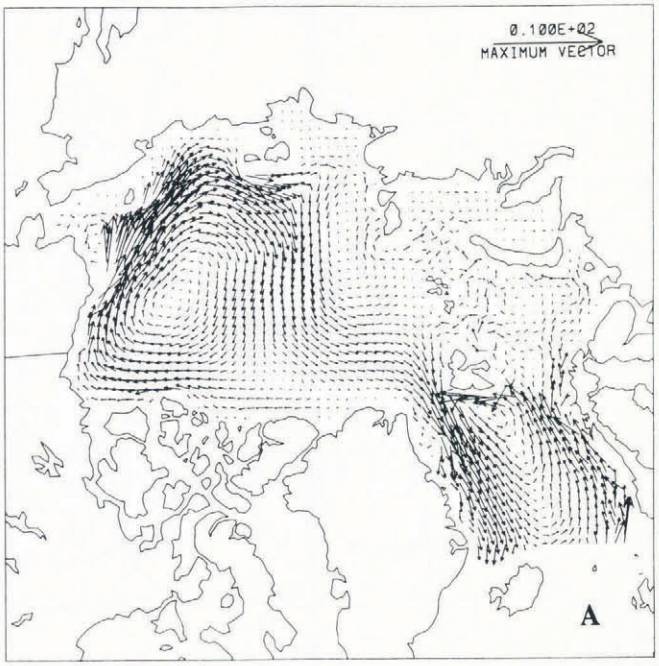

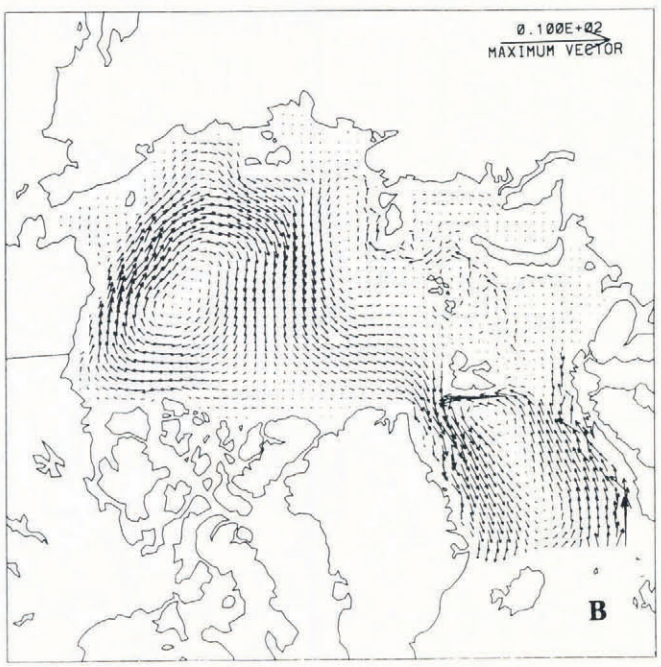

Fig. 3. (a) March and (b) August 1981 ocean velocities, 80 km standard simulation.

Table 1. Mean annual point values of the stream function (in Sverdrups) at selected points in each of the major basins. The selected points are denoted by an "x" in Figure 1.

Model	Stream-function characteristics		
	Canadian Basin (Sverdrups)	Eurasian Basin (Sverdrups)	GIN seas (Sverdrups)
160 km Std.	1.7	0.7	1.1
80 km Std.	3.0	2.8	4.5
80 km Low Visc.	2.9	3.5	4.8
80 km High Visc.	2.7	1.8	4.1

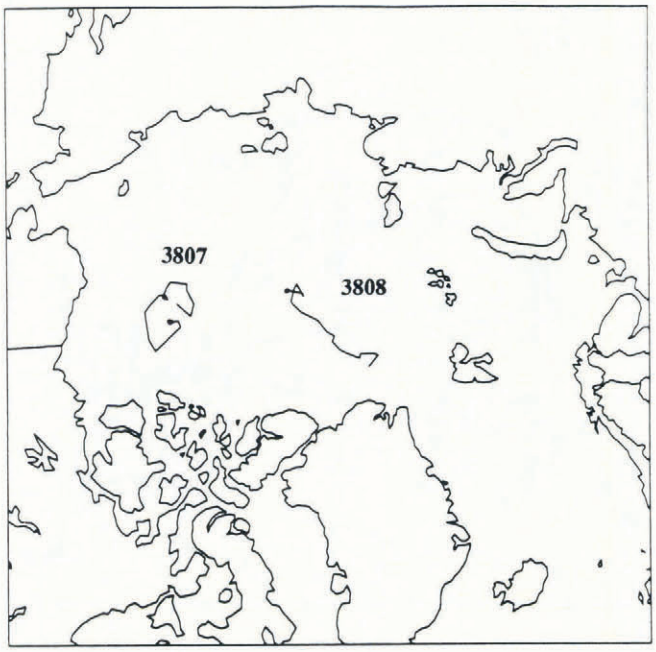

Fig. 4. Plot of observed buoy tracks in relation to the Arctic Basin. The time period observed was June 1981 to December 1982.

Point values of the mean annual stream-function for each of the three major basins are presented in Table 1 for each of the models. The point at which each average was taken is denoted by an "x" in Figure 1, and was obtained by finding the maximum local value of the three-year mean annual stream-function in each of the models. A comparison of the 160 km and the high viscosity 80 km simulation, which use the same viscosity, demonstrates the increase in circulation resulting from the increase in resolution. The circulation in the Eurasian Basin is most sensitive to changes in both viscosity and resolution. Lesser effects are reflected in the GIN seas, with the Canadian Basin region least sensitive to these changes. The overall conclusion here is that, in order to obtain the counter-clockwise circulation in the Eurasian Basin consistently, both high resolution and low damping are required (such as in the 80 km standard model).

In order to begin to compare the effectiveness of the models in predicting ice-drift characteristics, comparisons of the model runs were made with observed buoy drifts during the latter half of 1981 and the first half of 1982. Figure 4 presents the locations of these observed drift tracks within the Arctic Basin. Figure 5 presents the plots of two of the actual buoy tracks, combined with the predicted drift-tracks produced by the 80 km standard simulation, the 160 km standard simulation, and the ice-only simulation. The two buoy tracks were chosen to represent different regions of the Arctic Basin, with buoy 3807 located in the Beaufort Gyre and buoy 3808 in the Transpolar Drift Stream. These two tracks are representative of the results obtained. The observed tracks were obtained from twice-monthly latitude and longitude locations of the buoys. The simulated tracks were obtained by adding vectorially the simulated ice-drift vectors produced by the models at the buoy location. The horizontal and vertical axes in the plots represent the drift of the buoy in the simulation grid in a scale of kilometers.

https://doi.org/10.3189/1991AoG15-1-552-162 Published online by Cambridge University Press

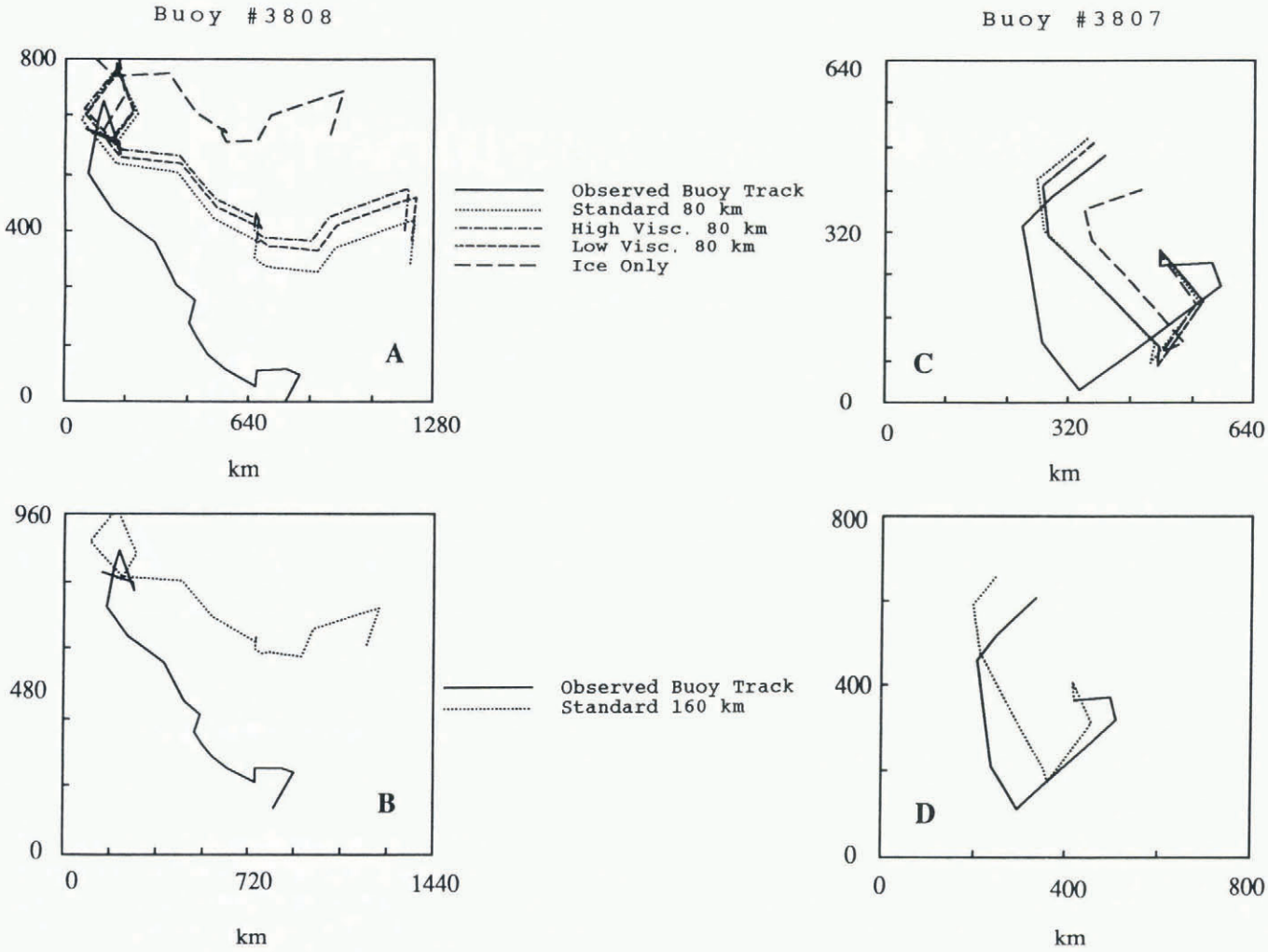

Fig 5. (a) Plot of predicted track for buoy 3808, 80 km simulations. (b) Plot of predicted track for buoy 3808, 160 km simulation. (c) Plot of predicted track for buoy 3807, 80 km simulations. (d) Plot of predicted track for buoy 3807, 160 km simulation. The predicted values represent monthly average simulated velocities interpolated to the buoy position and then plotted on a progressive vector diagram.

Although the differences between the 160 km and 80 km ice-drift simulations were small, both show a marked contrast to the ice-only simulation, representing the improvement provided by the addition of ocean currents to the ice-drift predictions. However, in comparisons of buoy drift near the Siberian Shelf in the region of maximum current variations (Fig. 3), the 160 km model exhibits a much closer correlation to observed buoy drift than do the 80 km simulations. As mentioned earlier, this feature is likely to be due to the exacerbation of the poor vertical resolution along the Siberian Shelf by the increased horizontal resolution. Note that the effect of viscosity on ice drift does not seem to be significant. The ice-drift results for the region covered by the Transpolar Drift Stream indicate a problem with the turning angle, which is possibly another by-product of the poor simulation of the West Spitsbergen Current. In particular, we speculate that significant inflow through the Fram Strait might help direct the East Greenland Current towards Greenland, which is more in line with the observed buoy track. It is also possible that this feature may represent inadequacies in the Levitus "observed" temperature and salinity fields.

Ice margin characteristics

Of particular concern to climate studies is the interannual variation in ice extent, as well as the physical mechanisms responsible for this variation. Figure 6 compares the three-year simulated February ice edge of the standard 160 km and 80 km models to the observed February ice edges. As can be seen, the simulated ice extents in the 160 km model are consistently larger than the observed ice extents, especially in the Barents Sea region. The 80 km simulated ice edge, on the other hand, slightly underestimates the ice edge in the Barents Sea while still somewhat overestimating the ice extent in the Greenland Sea. Both simulations, however, reproduce the interannual cycle in the Barents Sea. Specifically, a greater ice extent in 1982, followed by a significant decrease in ice extent in 1983, is simulated, consistent with the observed data. Overall, the 80 km model most accurately reproduces both the observed ice edge and the interannual variability and simulates well the ice edge in the region between Svalbard and Novaya Zemlya. In the Greenland Sea, on the other hand, excessive ice build-up occurs on the north coast of Iceland in the model results for both the 80 and 160 km models.

The seasonal and interannual ice-margin variations

https://doi.org/10.3189/1991AoG15-1-552-162 Published online by Cambridge University Press

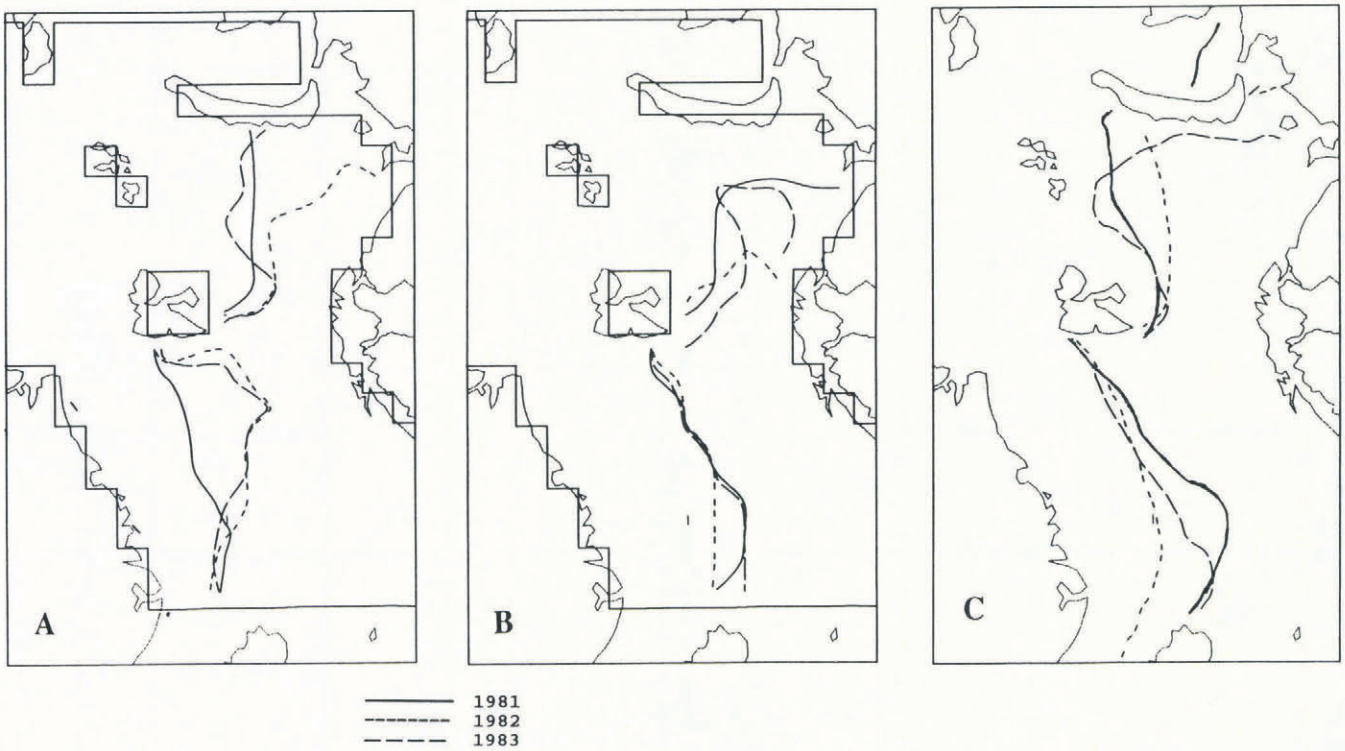

Fig. 6. (a) 1981–83 observed February ice margins. (b) 1981–83 February ice margins, 160 km standard simulation. (c) 1981–83 February ice margins, 80 km standard simulation.

are tied closely to the strength of the ocean circulation and the concomitant oceanic heat fluxes. In particular, analysis of the integrated flow in the region of the Greenland and Barents seas shows a decrease in integrated flow between 1981 and 1982 and an increase between 1982 and 1983. This feature is evident in a time-series of the stream-function taken at a point at the southern margin of the analysis region (Fig. 1) in the GIN and Barents seas (Fig. 7). In the Barents Sea, this increased circulation manifests itself as a more northward penetration of ocean flow. For example, during the winter months, an examination of stream-function variation in the Barents Sea region shows a larger vertically integrated flow further north between Franz Josef Land and Svalbard during 1982, with an increased flow between Franz Josef Land and Novaya Zemlya in 1983.

The change in the integrated flow is also reflected strongly in the seasonal cycle of the heat flux (integrated over the region enclosed in solid lines in Fig. 1) for the same months (Fig. 8). The ice-edge response to this variation is evident in the interannual variation in the ice edge in Figure 6c, exhibiting an advancing margin from 1981 to 1982 and a retreating margin from 1982 to 1983. Although showing less ice extent than observed, due to the excessive flow into the Barents Sea, these results suggest a very direct correlation between the barotropic circulation and the northward heat transport and the ice-edge variation. Specifically, the results suggest that an increased northward flow results in increased oceanic heat flux and a retreating ice margin. Note also, with respect to resolution, an increase in circulation in the GIN seas from 2 Sverdrups in the 160 km simulation to 4 Sverdrups in the

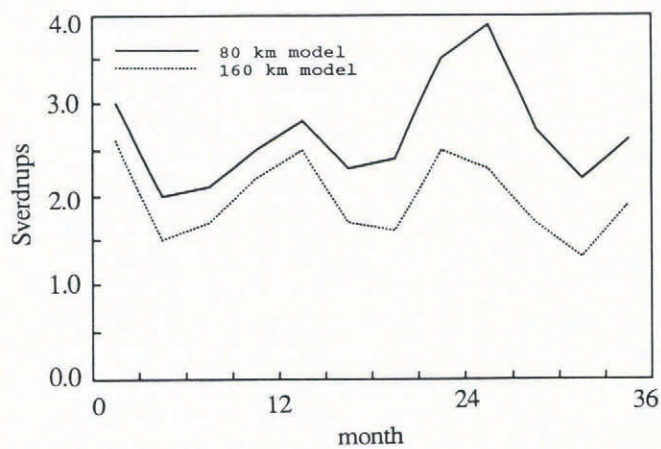

Fig. 7. Time-series of the stream-function at the southern boundary of the GIN seas. Location where the time-series was taken is marked by an "x" in Figure 1.

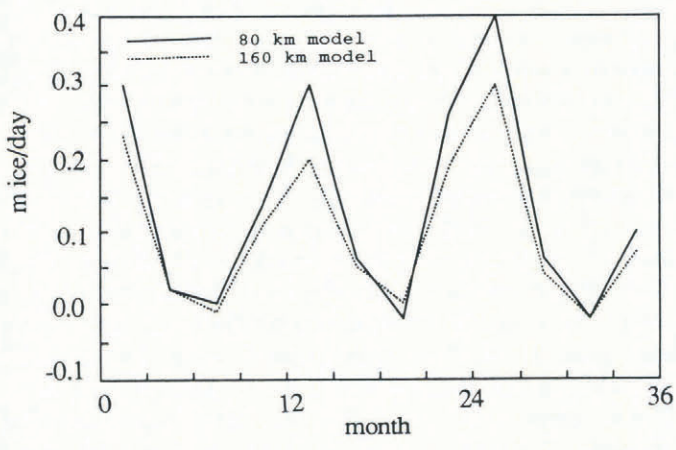

Fig. 8. Seasonal cycle of oceanic heat flux into the mixed layer, averaged over the GIN and Barents seas (denoted by an outlined area in Fig. 1).

https://doi.org/10.3189/1991AoG15-1-552-162 Published online by Cambridge University Press

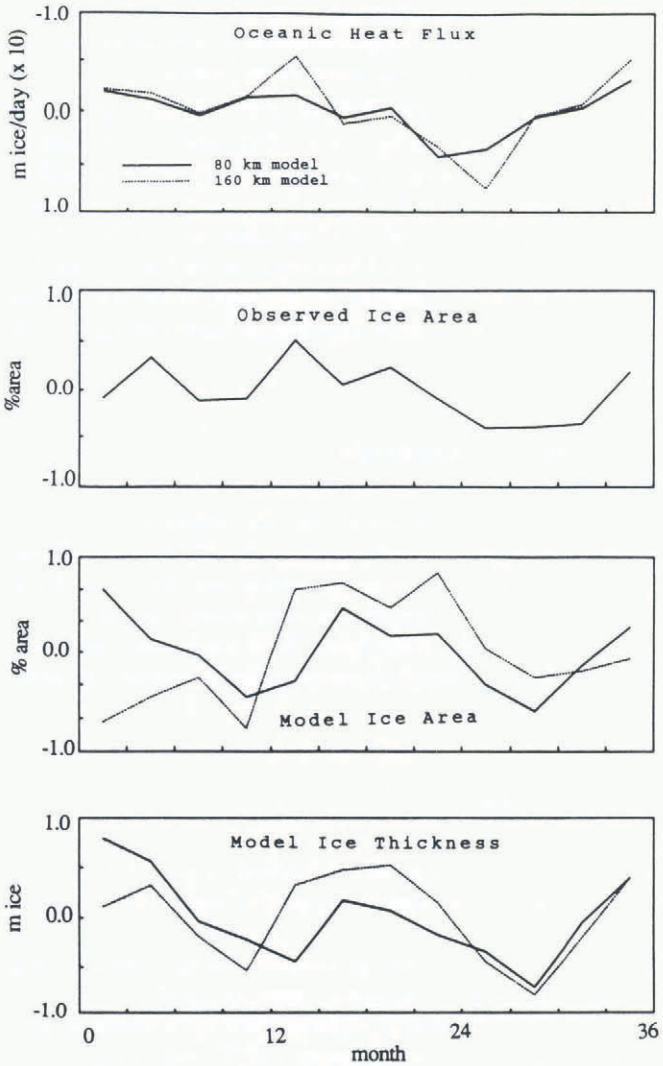

Fig. 9. Interannual variation (averaged over the GIN and Barents seas) of oceanic heat flux, modelled ice concentration and modelled ice thickness versus the interannual variation of observed ice concentration.

80 km simulation, providing an increase of one-third in the heat flux.

To obtain more temporal detail, a plot of the interannual variations of heat flux, modelled ice concentration, and modelled ice thickness (summed over the region denoted in Fig. 1) for the 160 and 80 km standard models is presented in Figure 9 in comparison to observed ice concentration. Figure 10 shows the full variability of the ice margin without the seasonal cycle removed. Table 2 presents the correlation coefficients for each of the interannual curves in Figure 9 versus the observed ice concentration. Correlation coefficients are provided for the ice-only data (not plotted) as a comparison for the improvement provided by the full model. Figure 9 and Table 2 show that, whereas the two ice–ocean simulations do not seem to exhibit a significant difference in correlation, they are both significantly better than the ice-only case, where there is a negative correlation caused by the removal of interannual variation in the heat flux. Moreover, although the correlations are similar, an examination of the full seasonal cycle of ice concentration

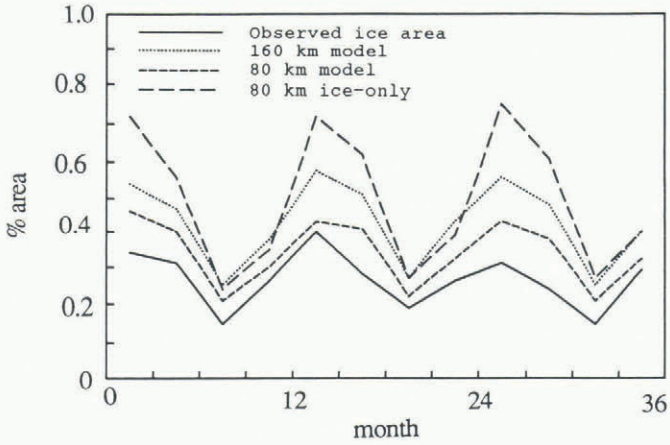

Fig. 10. Seasonal cycle of ice concentration for the 80 km-standard, 160 km-standard and ice-only models versus observed ice area, averaged over the GIN and Barents seas.

(Fig. 10) shows that the 80 km simulation exhibits a considerable improvement over both the 160 km and ice-only simulations in terms of the magnitude of ice extents in the simulations. However, the 80 km results still produce more ice than observed due to the excessive build-up along the north coast of Iceland.

With regard to the interannual variabilities, the main physical point shown by the above result is that stronger winds tend to increase the ocean circulation (and hence heat flux), which causes a retreat of the ice edge. With an ice-only model, on the other hand, stronger winds can lead to greater ice growth and extent. Concerning the seasonal cycle, the more robust circulation in the 80 km model does improve the overall ice margin. However, remaining excessive ice along East Greenland suggests that the oceanic boundary layer processes are not treated adequately.

CONCLUDING REMARKS

The general trend of results presented here is consistent with the important influence that oceanic heat exchange in the Greenland, Iceland and Norwegian seas has on the variability of the ice edge, both on seasonal and interannual time-scales. In particular, the magnitude of the integrated flow in both the 80 and 160 km models correlates well with the interannual variation in the ice edge. However, the 80 km resolution model has a significantly stronger circulation in the Greenland Sea than the 160 km model and also has a more realistic

Table 2. Correlation coefficients for the interannual variation of oceanic heat flux, ice concentration and ice thickness for the 80 km and 160 km models versus observed ice concentration

Parameter	80 km	160 km	Ice-only
Heat flux	0.51	0.64	–
Ice compactness	0.32	0.32	−0.29
Ice thickness	0.33	0.79	−0.35

https://doi.org/10.3189/1991AoG15-1-552-162 Published online by Cambridge University Press

seasonal cycle. Whereas this increased circulation allows the magnitude of the seasonal and interannual variation in the Barents Sea itself to be modelled well, the simulated ice edges in the 80 km model do not extend as far south as the observed ice margins. This feature is likely to be due to lack of flow through the Fram Strait, which, coupled with more robust flow in the 80 km model, leads to somewhat excessive flow through the Barents Sea region.

The ocean circulation is most sensitive to changes in resolution, although the integrated stream-function exhibits a small but discernible response to variations in viscosity. The exception to this is the circulation in Eurasian Basin, which exhibits significant variations in response to viscosity changes. Due to the low vertical resolution, which in shallow areas requires at least three levels for a minimum of 140 m, problems arise in the ocean circulation which limit the ability of the model to simulate the ice-drift and ice-edge variations accurately. The effect of this is most pronounced in the currents over the Siberian Shelf. Perhaps the largest difficulty is the poor simulation of the West Spitsbergen Current. This causes a redirection of flow into the Barents Sea, producing a slightly recessed ice margin due to the increased heat transport into the region. Also, the East Greenland Current exhibits a slightly abnormal flow, directed against the west coast of Svalbard, before flowing south through the Fram Strait. Therefore, the buoy-drift results in the Transpolar Drift Stream have a direction inconsistent with observed drift, although the pattern of drift is the same throughout the period of simulation. Overall analysis of the simulated drift predictions indicate that changes in viscosity and horizontal resolution provide no major improvement to ice-drift predictions.

A dominant result of the simulation reported here is a substantial increase in the strength of the circulation in the Greenland–Norwegian sea as the resolution is increased from 160 to 80 km. This increased circulation results in more northward heat transport, with a concomitant decrease in ice extent in the relatively shallow Barents Sea. However, despite this more robust circulation, the ice extent in the Greenland–Iceland sea is still extensive. Whereas some of this deficiency may be due to too much warm Atlantic water flowing northward into the Barents Sea, rather than returning southward, it is more likely that inadequacies in the boundary layer formulation in the ocean model are responsible for excessive ice extent. In particular, a boundary layer formulation including penetrative convection is probably necessary to simulate the dominant physical processes in the Greenland Sea region adequately. With the inclusion of the boundary layer formulation and the resolution of problems with the West Spitsbergen Current, it is hoped that the 80 km model will provide more significant improvements over the 160 km model.

ACKNOWLEDGEMENTS

We would like to acknowledge the invaluable help of several people in the completion of this paper: Peter Ranelli for help with the numerical model, Jim Waugh for general computer consultation, and Jinlun Zhang for the interpolation of the data fields. This work was supported by the Office of Naval Research under contract number N00014-86-K-069.

REFERENCES

Bryan, K. 1969. A numerical method for the study of the circulation of the world oceans. *J. Comput. Phys.*, **4**, 347-376.

Hibler, W.D., *III*. 1979. A dynamic thermodynamic sea ice model. *J. Phys. Oceanogr.*, **9**(4), 815-846.

Hibler, W.D., *III*, and K. Bryan. 1987. A diagnostic ice–ocean model. *J. Phys. Oceanogr.*, **17**(7), 987-1015.

Levitus, S. 1982. *Climatological atlas of the world ocean. NOAA Prof. Pap.* 13.

Semtner, A.J., *Jr.* 1987. A numerical study of sea ice and ocean circulation in the Arctic. *J. Phys. Oceanogr.*, **17**(8), 1077-1099.

The accuracy of references in the text and in this list is the responsibility of the authors, to whom queries should be addressed.